ELSEVIER

Marine Geology 173 (2001) 121–139

MARINE GEOLOGY
INTERNATIONAL JOURNAL OF MARINE GEOLOGY, GEOCHEMISTRY AND GEOPHYSICS

www.elsevier.nl/locate/margeo

# Intertidal beach slope predictions compared to field data

A.J. Madsen, N.G. Plant*

*Faculty of Technology and Management, University of Twente, WB-Bldg, P.O. Box 217, 7500 AE Enschede, The Netherlands*

Received 20 June 2000; accepted 19 December 2000

**Abstract**

This paper presents a test of a very simple model for predicting beach slope changes. The model assumes that these changes are a function of both the incident wave conditions and the beach slope itself. Following other studies, we hypothesized that the beach slope evolves towards an equilibrium value that depends nonlinearly on wave steepness ($H/L$). The rate of beach slope response is assumed to depend on both the degree of slope disequilibrium and on the incident wave energy. The model was tested against daily beach slope observations derived from digital images of the nearshore zone. Approximately, $10^4$ images were analyzed over eight, mostly consecutive, month-long periods along a 2 km length of beach. The slope change model was calibrated by fitting it to the daily differences in the alongshore-averaged slopes, which were obtained from a 500 m (alongshore) subset of the observations. An equilibrium slope prediction proportional to the wave steepness ($H/L$) raised to the $-1$st to $-2$nd power performed best compared to several alternative models. The response rate of beach slope changes depended on the wave height, raised to the 3rd or 4th power. A characteristic response time for the system was found to be 1–2 days. The calibrated (i.e. hindcast) model explained 30–40% of the observed slope change variance, indicating that the model was consistent with the data. However, when the model was used to predict the evolution of the beach slope time series (i.e. to forecast), the prediction error variance was equal to or only slightly lower than the observed temporal variability in the slopes. The present model is sufficiently accurate to characterize beach slope dynamics, but its predictive capability would not outperform a model that predicts a constant, mean slope. 

*Keywords*: Video images; Equilibrium; Hindcast; Forecast

## 1. Introduction

A fundamental variable that is used to characterize beaches is the shore normal slope. This variable is important because it governs the behavior of incident waves as they shoal and break. Battjes (1974) used the non-dimensional Iribarren number, $\xi = \beta\ (L/H)^{1/2}$ (where $\beta$ is the beach slope, $L$ the wave length (typically evaluated in deep water), and $H$ is the wave height (typically evaluated at the onset of breaking) to describe the beach steepness. If $\xi < 1$, then a beach is hydrodynamically flat, and waves will dissipate much of their incident-frequency energy in wave breaking (Thornton, 1979; Guza and Thornton, 1985). If $\xi > 1$, waves will tend to be reflected by the beach. Because waves drive sediment transport and the beach influences the waves (e.g. via the slope), there is strong feedback associated with any beach change.

It is important to understand how the feedback between the waves and the beach topography affect beach change. Practical reasons for understanding these changes stem from coastal protection and management needs. Often, interest focuses on the

* Corresponding author. Present address: Naval Research Lab., Code 7440.3 (bldg. 2438), Stennis Space Center, MI 39529, USA.
*E-mail address:* n.plant@nrlssc.navy.mil (N.G. Plant).

0025-3227/01/$ - see front matter 
PII: S0025-3227(00)00168-7

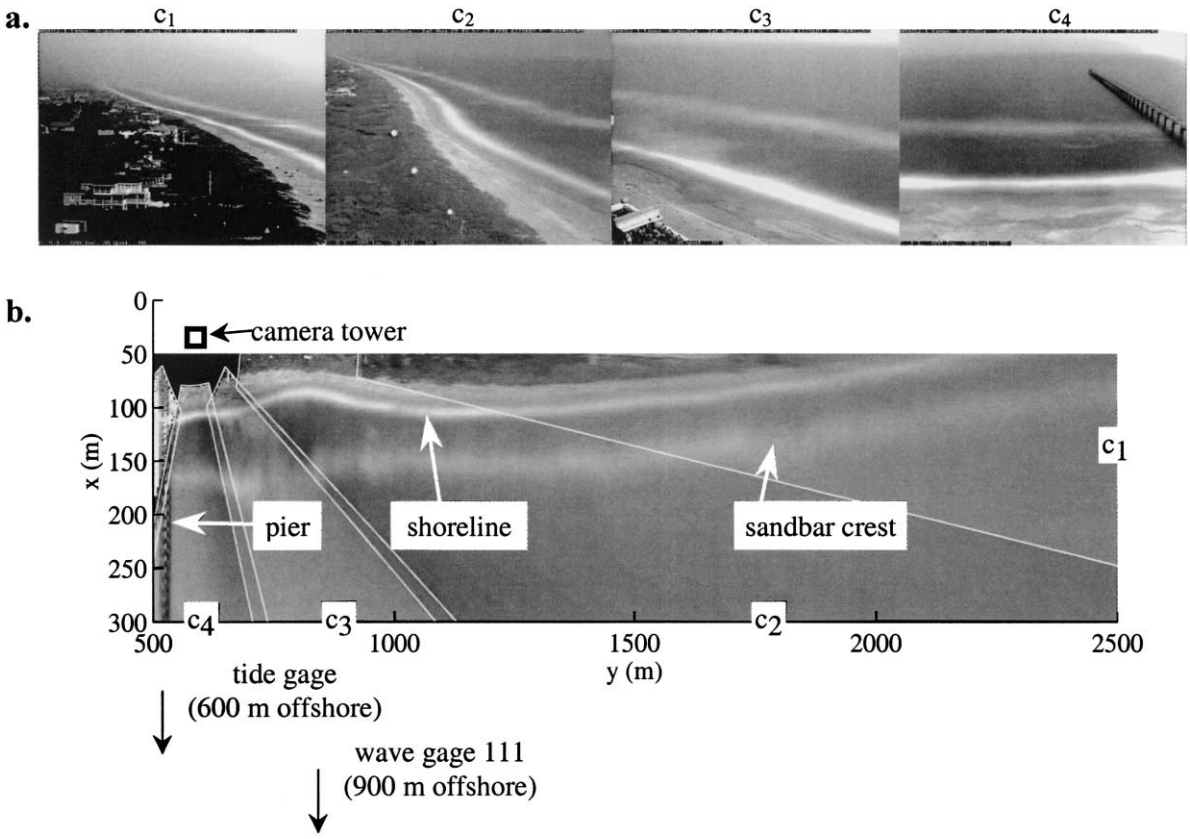


Fig. 1. (a) Oblique images used to generate, (b) plan image, 1400 GMT, 29 August 1998.

intertidal beach slope, where we can witness directly the interaction between beach and wave dynamics. If the subaerial beach loses or gains sand, this sand must have passed the intertidal zone. (We ignore the contribution of aeolian sediment transport.)

The sediment transport processes operating in the intertidal zone are driven by tidal and swash variations. These processes are complicated and difficult to model. Also, these processes are difficult to sample because they occur in an energetic and rapidly changing environment. In spite of the complexity of this system, it appears to possess some stability mechanism, such that the beach slope, averaged over many swash or tide cycles, may reach an equilibrium value with respect to the wave forcing. This suggests that beach slope variations may be predictable.

The most frequently cited predictions of the intertidal (or swash) slope are primarily based on observed geographic variability of beaches (Bascom, 1954). Clearly, the shape of beaches is strongly controlled by geologic variables, such as grain size, grain shape, and grain density, and rate of sediment supply. The geologic environment also influences the hydrodynamic regime. The tidal range depends on the shape and orientation and geographic location of the coastline, and wave conditions depend on the ocean basin that is the source of wind waves.

Many empirical relationships between beach slope, grain size, and wave climate have been published. Komar (1998, pp. 285–290) summarizes these models. There is a clear trend of steepening of the shoreline beach slope with increasing grain size, even when data from beaches with very different incident wave energy are compared (Bascom, 1954). When comparing beaches that are composed of similar grain size, the beach slope is generally flatter as the average wave energy increases and predicted slopes are steeper as wave period (or, equivalently,

wave length) increases. In general, the beach slope predictions have the form (see Sunamura, 1984 and references therein)

$$\beta_{eq} \propto a_2\left(\frac{H}{L}\right)^q D^r, \tag{1}$$

where $D$ is the grain size, $q$ and $r$ are constant exponents. $\beta_{eq}$ denotes either an equilibrium beach slope that depends on steady wave conditions or an average slope with respect to average wave conditions.

Most beaches experience significant variation in incident wave height and wave period. Models using the form of Eq. (1) were developed for hypothetical steady state conditions. It is not clear whether they can be used to predict the temporal variation of the beach slope. If we restrict our attention to a single location, then the grain size is relatively constant and we need only consider the relationship between the hydrodynamic variations and beach slope. We wish to determine if models such as Eq. (1) can be adapted to predict variation in beach slopes that are forced by variation in wave conditions.

In this paper, we test a model that predicts shoreline beach slope change. We use a set of eight, month-long time series of daily beach slope estimates obtained from hourly time-averaged images of a well-studied beach at Duck, NC (USA) (Holman and Sallenger, 1993) (Fig. 1). In Section 2, the model is developed to be consistent with the field test, which experienced constantly changing wave conditions. In Section 3, the data collection methods and resulting data set are described. In Section 4, the data are compared to the model predictions, which were driven by measured wave height and wave period. We discuss the implications of model–data comparison results in Section 5 and conclusions are presented in Section 6.

## 2. Theory

### 2.1. Simple models of nearshore morphodynamics

It is often assumed that a particular set of incident wave conditions is associated with a corresponding, stable equilibrium state of the beach. That is, if wave conditions were steady, a beach would asymptotically approach a single state, independent of the initial state. This hypothesis has been tested previously, in association with 'morphodynamic state' models (Wright and Short, 1984; Wright et al., 1985). Wright and Short's (1984) morphodynamic state model suggests that the shape of the surf zone bathymetry tends towards one of six forms, ranging from dissipative (unbarred and alongshore uniform) to reflective (bars welded to shore and significant alongshore irregularity). To predict beach state variability in time, Wright et al. (1985) hypothesized that the direction of beach state change (i.e. towards more dissipative or more reflective) would depend on the instantaneous disequilibrium. Their predictive model had the form

$$\frac{\mathrm{d}}{\mathrm{d}t}S(t) = a + b[\Omega(t)]^{\mathrm{p}}[S(t) - S_{eq}(t)], \tag{2}$$

where $S$ is the beach state, $S_{eq}$ the predicted equilibrium state (a function of wave conditions), and $a$ and $b$ are constant coefficients. The term $\Omega^{\mathrm{p}}$ is a rate function (depending on the 'Dean Parameter' $\Omega = H/[wsT]$, where $H$ is the wave height, $w_s$ is the sediment fall velocity, and $T$ is the wave period (Dean, 1973; Kriebel and Dean, 1993)). The rate function characterizes the response time of the morphologic model. This beach state model (2) was compared to observed beach state changes and synchronous measurements of wave conditions. The model was shown to agree qualitatively with the observations.

Plant et al. (1999) used a similar model to predict cross-shore migration of sandbars. In this case, the beach state was described by the cross-shore position of a sandbar and the predictive equation took the form

$$\frac{\mathrm{d}}{\mathrm{d}t}X(t) = a_1[H(t)]^3[X(t) - X_{eq}(t)], \tag{3}$$

where $X$ is the time-varying bar position and $X_{eq}$ is an equilibrium position that depended on the time-varying wave height. This model was compared to monthly observations of sandbar position, and was shown to have significant predictive skill over periods of nearly a decade.

Here, we develop and test a similar model for beach slope prediction, having the form

$$\frac{\mathrm{d}}{\mathrm{d}t}\beta(t) = a_1 H(t)^{\mathrm{p}}[\beta(t) - \beta_{eq}(t)], \tag{4}$$

where $\beta$ is the shore-normal beach slope and $a_1H^{\mathrm{p}}$ is assumed to be an appropriate rate function.

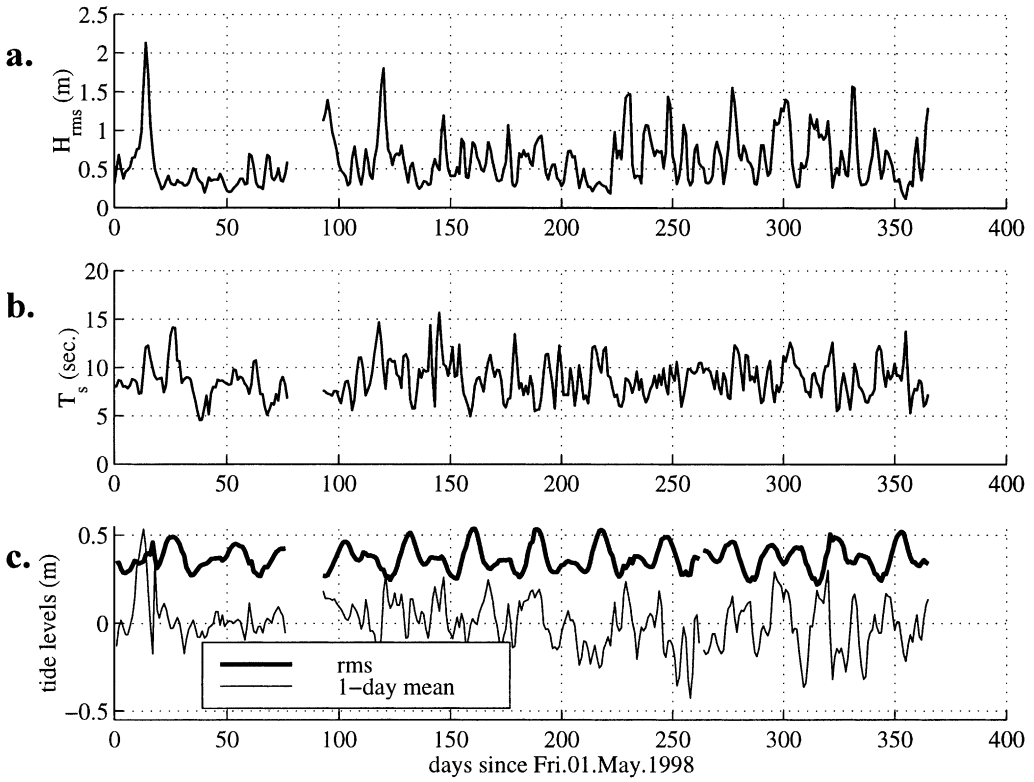


Fig. 2. Time series of daily-averaged hydrodynamic properties. (a) Wave height and (b) wave period measured at gage 111 (8 m water depth). (c) The daily mean tidal level and daily rms tide level (i.e. an indication of daily tide Range) measured at pier-end wave gage.

### 2.2. Equilibrium beach slope model

A number of studies have developed empirical relationships for predicting the equilibrium slope in terms of the wave steepness, as in Eq. (1). Experiments in a wave flume containing sand of 0.22 mm diameter by *Rector* (see citation in Komar, 1998, p. 287) found that the foreshore slope above the still water level depended on the deep-water wave steepness according to the relationship

$$\beta_{eq} = 0.30\left(\frac{H_\infty}{L_\infty}\right)^{-0.3}, \tag{5}$$

where $H_\infty$ and $L_\infty$ are deep water wave heights and wave lengths. This model indicates that the greater the wave steepness, the lower the beach slope. Using regression analyses on field data, Harrison (1969) found a similar inverse relationship between the beach-face slope and wave steepness.

Attempts have been made to relate the beach-face slope to a variety of other dimensionless parameters that incorporate measures of wave height and period as well as sediment size. Dalrymple and Thompson (1976) employed the Dean number, $\Omega$. From the physical arguments of Dean (1973), this ratio is a measure of whether a sediment particle lifted into suspension by a passing wave can fall to the bottom again before the next wave cycle. Also, Sunamura (1984) studied empirical relationships for the beach slope from both laboratory and field data. The laboratory data were described by

$$\beta_{eq} = 0.013\left(\frac{H_b}{g^{1/2}T}\right)^{-2} D + 0.15, \tag{6a}$$

where $H_b$ is the breaking wave height and $D$ the grain size. The field data were described by the equation

$$\beta_{eq} = 0.12\left(\frac{H_b}{g^{1/2}T}\right)^{-0.5} D^{1/4}. \tag{6b}$$

According to these results, laboratory beaches are predicted to be steeper than natural beaches under similar wave steepness conditions. This points to severe problems of extrapolation from laboratory experiments to field conditions. It is not clear why the exponents differ in the formulations for Eqs. (6a) and (6b), and why the offset at high wave steepness (e.g. $\beta_{eq} \rightarrow 0.15$) exists in Eq. (6a), but not in Eq. (6b). Inspection of the data suggests that a single model with adjustable coefficients would have described sufficiently both laboratory and field data.

We propose to generalize the equations for the equilibrium slope presented so far, representing them with the form given in Eq. (1). Our assumption is that, aside from grain size dependence, the equilibrium slope is a function of wave steepness, $H/L$, where linear wave theory relates the deep water wave length to wave period ($L = gT^2/2\pi$). We assume that the equilibrium slope may be given by

$$\beta_{eq} = a_2\left(\frac{H}{L}\right)^q. \quad (7)$$

Inserting this form into Eq. (4) closes the slope prediction model. We can compare this model to field observations of beach slope, offshore wave height, and wave period. We expect that the exponent $p$ in Eq. (4) is in the range 1–4, $q$ in the range $-0.3$ to $-2$, and that $a_1$ and $a_2$ will depend strongly on the grain size.

## 3. Data description

### 3.1. Duck, NC, field site

Field measurements of nearshore bathymetry and hydrodynamic conditions at Duck have been sampled continuously by researchers at the Army Corps of Engineers Field Research Facility (FRF) since 1980. Wave conditions are sampled along a 500 m research pier and at several offshore stations. We utilized observations sampled every 3 h from a gage located in 8 m mean water depth (gage 111 — see Fig. 1b). The rms wave height during our study period (May 1998–April 1999) varied from 0.1 to 3.7 m and the significant wave period varied from 3 to 18 s (Fig. 2a and b shows daily averages). Water levels (Fig. 2c) were sampled every 6 min at the pier end. Observed values fell between $-1.2$ and 1.6 m (referenced to national geodetic vertical datum of 1929 — NGVD29), and the tidal elevation mean and standard deviation were 0.2 and 0.4 m.

The bathymetry at Duck has been surveyed bi-weekly to monthly along several profiles that span 1 km alongshore, centered about the research pier (Birkemeier and Mason, 1984; Birkemeier 1985.). The temporal sampling rate is not frequent enough to resolve variations in beach slope at the shore, which have a response time of several days (Miller et al., 1989; Holland and Holman, 1996). However, the directly surveyed bathymetry is useful to our analysis as a means of spot-checking remotely sampled bathymetry.

Grain sizes at Duck vary along the cross-shore profile, ranging from a relatively coarse shell 'hash' of 2.0–0.5 mm in the swash zone to finer 0.1 mm sand in 8 m depth (Birkemeier et al., 1985; Nichols et al., 1998). We lack detailed descriptions of temporal and spatial variation in grain size, which could be incorporated into the beach slope model, as in Eq. (1). In order to proceed with testing the present model, we are forced to neglect grain size variations. Subsequent model–data mismatch could be attributed to this omission, which could be serious in light of the wide range of observed grain sizes.

### 3.2. Beach slope observations

Digital video images of the surf zone at Duck, NC have been collected since 1986, and have been used to describe nearshore sandbar variability (Lippmann and Holman, 1989, 1990; Lippmann et al., 1993) and shoreline variability (Plant and Holman, 1997a,b). These images are obtained from cameras that are mounted at an elevation of 44 m above mean sea level on a tower, which is positioned, approximately, 75 m landward of the shore (Fig. 1b). There are currently seven cameras that provide a 180° view of the nearshore region.

In this study, we will utilize time-exposure images from four camera views to the north of the research pier (Fig. 1a). The images were collected approximately hourly between 1 May 1998 and 31 April 1999. Each digital image recorded the relative light intensities on an integer scale from 0 (black) to 255 (white) at 640 horizontal and 480 vertical, equally

spaced pixel coordinates. Some images recorded color information, which we mapped to a gray scale.

Under some conditions, swash motions at the shoreline generate foam, which produces a distinct shore-parallel band of high light intensity in time exposure images (Fig. 1). Plant and Holman (1997b) (hereafter referred to as PH97) name the bright band the shoreline intensity maximum (SLIM). Changes in the SLIM position are correlated to changes in the still water level. As the tide rises and falls, the SLIM moves onshore and offshore, visually marking beach elevation contour lines. PH97 mapped beach topography by identifying SLIM contour lines and then assigning the measured tidal elevation to them. The rms elevation error of this technique was about 10 cm, after removing an offset bias. This error level is comparable to direct bathymetric survey error.

### 3.2.1. Plan images

To analyze the images in a geographic reference frame, oblique image intensities were mapped onto a horizontal plane. The spatial extent of the field area was defined on a regularly spaced grid: $\{y_j, x_k\} = \{y_0 + (j-1)\Delta y, x_0 + (k-1)\Delta x\}$, where $y_0 = 550$, $\Delta y = 5$ m, $x_0 = 50$, $\Delta x = 1$ m, and $y_j$ and $x_k$ are the sample spatial coordinates in the alongshore and cross-shore directions ($j = 1, 2, \ldots, 401$, and $k = 1, 2, \ldots, 251$). The alongshore extent of the field area was chosen to be within a region where the horizontal pixel resolution adequately resolved the intertidal region of the beach. At the greatest distance from the camera ($y = 2500$ m), the pixel resolution was 0.6 m in the cross-shore direction and 25 m in the alongshore direction.

We generated one plan image each hour. When possible, a single plan image was generated from oblique images obtained from all four cameras that spanned the field area. The oblique images that were available within a half-hour of each plan image sample time were mapped to a plane defined by the mean of the tidal elevations that were measured over the oblique image collection period. Because not all images were collected synchronously, tidal variation introduced an error into the mapping. The rms tidal elevation difference from the mean elevation, computed from all 1-h sample intervals was 0.09 m (80% of all changes were less than this value) and the maximum difference (absolute value) was 0.20 m.

The oblique images, which had overlapping coverage of the field area, were combined in each plan image as follows:

$$I_{\text{plan}}(t_i, y_j, x_k) = \sum_{c=1}^{4} I_{\text{oblique}}(u_{ijkc}, v_{ijkc}, c)/N^{ijk}_{\text{overlap}}, \qquad (8)$$

where $t_i$ is a sample time, $c$ an index identifying a particular camera, $I_{\text{plan}}$ a plan image, and $I_{\text{oblique}}$ an oblique image. Oblique image intensities that mapped into the study area were contrast stretched and normalized to a range of 0–1 before averaging over the overlapping images ($N^{ijk}_{\text{overlap}} = 1$ or 2). The pixel coordinates corresponding to $i$th time, $j$th and $k$th grid coordinate and $c$th camera view are $u_{\text{ijkc}}$ and $v_{\text{ijkc}}$. The intensities from the appropriate image were interpolated to these non-integer pixel coordinates. The transformation between geographic co-ordinates ($t$,$y$,$x$) and image coordinates ($u$,$v$) is described by Holland et al. (1997), and requires knowledge of the orientation (tilt, azimuth, roll), field of view, and location of each camera. The orientation of each camera was estimated via nonlinear regression, which fit a set of standard photogrammetric equations to measured control point coordinates and measured camera location. Radial lens distortion was removed in the transformation.

PH97 demonstrated that short-scale alongshore variations (such as beach cusps) are not accurately resolved by the SLIM mapping method. Therefore, image intensities were band averaged within $\delta y$ (set to 25 m in our application) meters of each $y_j$. The filtered plan images were then sub-sampled at the alongshore locations given by $y_{j'} = y_0 + (2j' - 1)\,\delta y$ ($j' = 1, 2, \ldots, 40$). Hereafter, we drop the prime from $j'$, since we will refer only to the sub-sampled grid.

### 3.2.2. SLIM identification

The method of extracting the SLIM position was modified further compared to the method used by Plant and Holman (1997a), who fit a parabola to the intensities near the shoreline and used the maximum in the fitted function to define the SLIM position. Instead, we located the SLIM by fitting a superposition of quadratic and Gaussian-shaped functions to intensities along a cross-shore transect that included the entire intertidal zone. The intensity function that

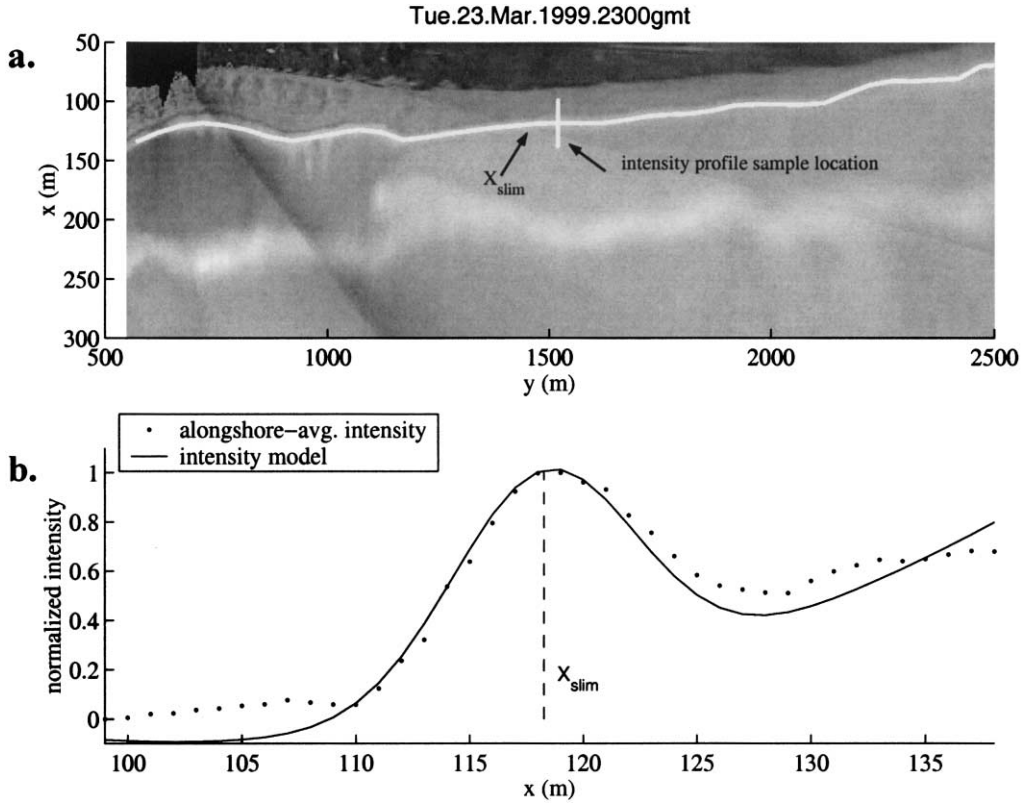


Fig. 3. Example SLIM position estimates corresponding to 23 March 1999 showing: (a) overlay of $X_{\text{slim}}$ (shore-parallel white line) on plan image, and (b) intensity profile at $y = 1500$ m. The intensity sample locations (shore-normal white line) are shown in (a).

we used was

$$\hat{I}(t_i, y_j, x) = I_0^{ij} + I_1^{ij} x + I_2^{ij} x^2 + A_{\text{slim}}^{ij} \exp\left[ -\left( \frac{x - X_{\text{slim}}^{ij}}{L_{\text{slim}}^{ij}} \right)^2 \right], \quad (9)$$

where $I_0, I_1, I_2$ parameterize the quadratic function and $A_{\text{slim}}$, $X_{\text{slim}}$, $L_{\text{slim}}$ parameterize the Gaussian function's amplitude, position, and width (Fig. 3). Compared to using the approach of PH97 to find the SLIM position, $X_{\text{slim}}$, our modification (Eq. (9)) provides additional means of interpreting the quality of each estimated shoreline position. For example, estimated $L_{\text{slim}}$ values that were too wide compared to the expected swash zone width indicated inconsistency of the SLIM estimate. Table 1 lists the criteria used to assess the quality of the observations. Details of the data quality control measures, which selected only a subset of the identified SLIM positions to use in the beach slope estimation, are presented in Appendix A.

The free parameters in Eq. (9) were adjusted to fit to the observed intensities in a least squares sense using an iterative Gauss–Newton search method. Each iteration was started with $I_0 = 10^{-4}$, $I_1 = 10^{-4}$, $I_2 = 10^{-4}$, $A_{\text{slim}} = 0.1$, and $L_{\text{slim}} = 5$ m. The SLIM position parameter, $X_{\text{slim}}$, was initialized with the output of a polynomial function of tide, time, and alongshore position

$$X_{\text{init}}(t_i, y_j) = c_0 + c_1 \eta(t_i) + \sum_{m=1}^{M_1} [(t_i)^m (c_{1+m})] + \sum_{m=1}^{M_2} [(y_j)^m (c_{1+M_1+m})], \quad (10)$$

where $\eta$ $(t_i)$ is the tide level at time $t_i$ and $c_m$ are function coefficients. The first coefficient is the

Table 1
Final SLIM selection criteria

| Criteria | Explanation |
|---|---|
| $L_{slim} > 2$ m | The data do not resolve small slim widths since $\Delta x = 1\ m$ |
| $L_{slim} < 20$ m | The typical width of intertidal zone at Duck was <20 m |
| $A_{slim} > A_{ci}$ | $A_{slim} > 0$ indicates that a Gaussian-shaped SLIM exists |
| $L_{slim} > L_{ci}$ | $L_{slim} > 0$ indicates that a Gaussian-shaped SLIM exists |
| $L_{slim} > X_{ci}$ | SLIM position error $< L_{slim}$ means position well estimated |
| $\lvert X_{slim} - X_{init}\rvert < 3Q_{adj}$ | $Q_{adj}$ is the rms deviation between the $X_{slim}$ estimates and a linear model prediction, which we call the adjacent-point prediction: $X_{adj}(t_i, y_j) = b_1 X_{slim}(t_i, y_j + 1) + b_2 X_{slim}(t_i,\ y_j - 1)$. Outliers were rejected and the parameters ($b_1$,$b_2$) were re-computed three times |

mean shoreline position. The second coefficient allows for tidal variation of $X_{init}$ on a beach with constant cross-shore slope equal to $1/c_1$. The remaining polynomial terms allow the initial SLIM position guess to vary with time ($M_1$ was 2) and alongshore ($M_2$ was 10). The purpose of this initialization function was to provide uniformly accurate initial guesses at all alongshore locations. (PH97 initialized each $X_{slim}$ search with alongshore-adjacent values, beginning with a pre-defined value at the first alongshore location. Estimation success at one location depended on success at other locations.)

The coefficients of Eq. (10) were estimated by fitting to all previously estimated $X_{slim}(t_i, y_j)$ values and corresponding tide levels before using Eq. (9) to extract the SLIM positions from a new image. These coefficients were estimated for the $n$th plan image via linear regression, which minimized a weighted square error: $Q_{init}(n) = \sum_{i,j} \{[X_{init}(t_i, y_j) - X_{slim}(t_i, y_j)]^2 W_{n,i,j}\}$. The weights were defined as

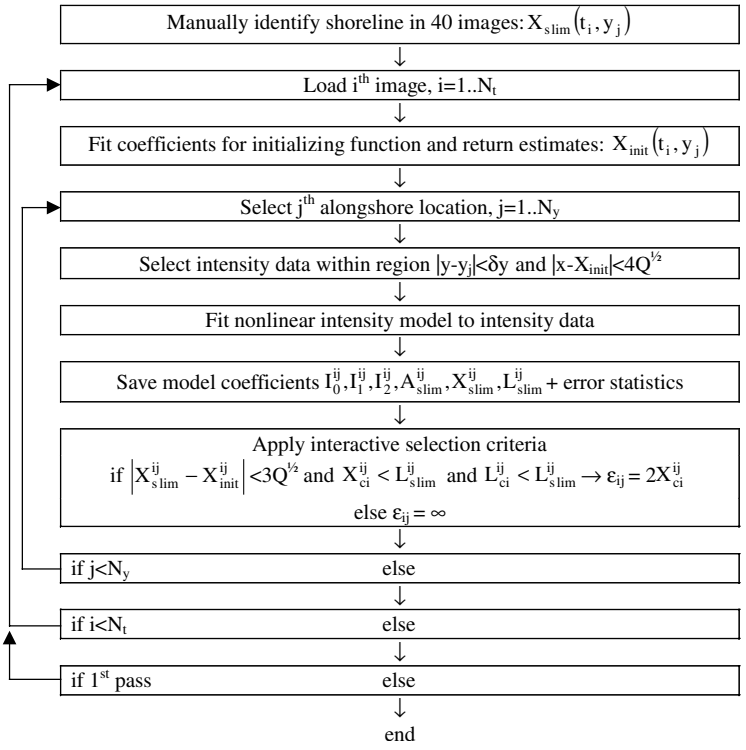


Fig. 4. Flow chart for extracting SLIM positions from plan images.

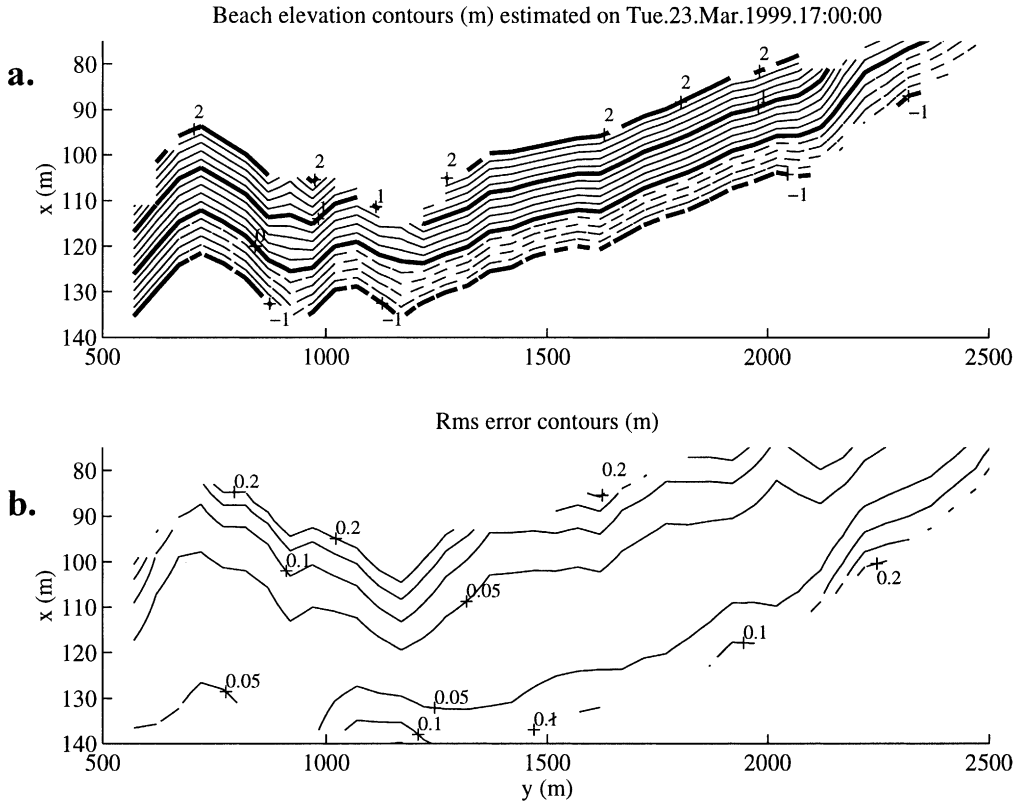


Fig. 5. Contours of: (a) beach elevation, and (b) elevation error estimates. These estimates are derived from SLIM data, sampled over ±3 day period, centered on 23 March 1999. Elevation contours appear only when the rms error is less than 0.1 m.

$W_{n,i,j} = 1/\epsilon_{ij}^2 \exp[-((t_i - t_n)/\delta t)]^2$. Each $\epsilon_{ij}$ was the expected root mean square error associated with each available $X_{\text{slim}}(t_i, y_j)$ estimate. The weights approach zero outside of a time window, $\delta t$ (14 days was used). The intensities used to constrain the parameters in Eq. (9) were sampled from a cross-shore Range that was chosen to be within four $Q_{\text{init}}^{1/2}$ of $X_{\text{init}}$, since this Range should include more than 99% of all $X_{\text{slim}}$ locations. Fig. 4 summarizes the steps taken to extract the shoreline position from the images.

### 3.2.3. Beach slope estimation

Measured tide levels and the corresponding SLIM positions (but only those that passed quality control standards: see Appendix A) were used to fit a series of articulated plates that represented the beach surface. Each beach plate was defined by its vertical intercept ($z_0$), and its slopes in cross-shore and alongshore directions ($\beta_x$, and $\beta_y$). These plates were assumed to vary in space and in time, such that, within the *ijk*th plate

$$Z_{\text{plate}}^{ijk}(x, y, t) = z_0^{ijk}(t) + (x - x_k)\beta_x^{ijk}(t) + (y - y_j)\beta_y^{ijk}(t), \tag{11a}$$

where the indices refer to an estimate centered on the *i*th time interval, *j*th alongshore position, and the *k*th cross-shore position. We omit the wave dependent elevation correction used by PH97, because this correction primarily introduced a constant vertical offset, which had little affect on the slope estimates.

The bathymetric plates described in Eq. (11a) were fit to the SLIM position and tide data by assuming that the beach varied slowly over a sample period that included several tidal cycles. Slow variation of the beach plate parameters was expressed in terms of a truncated Taylor series expansion about $t_i$:

$$z_0^{ijk}(t) = \hat{z}_0^{ijk} + (t - t_i)\dot{z}_0^{ijk}, \tag{11b}$$

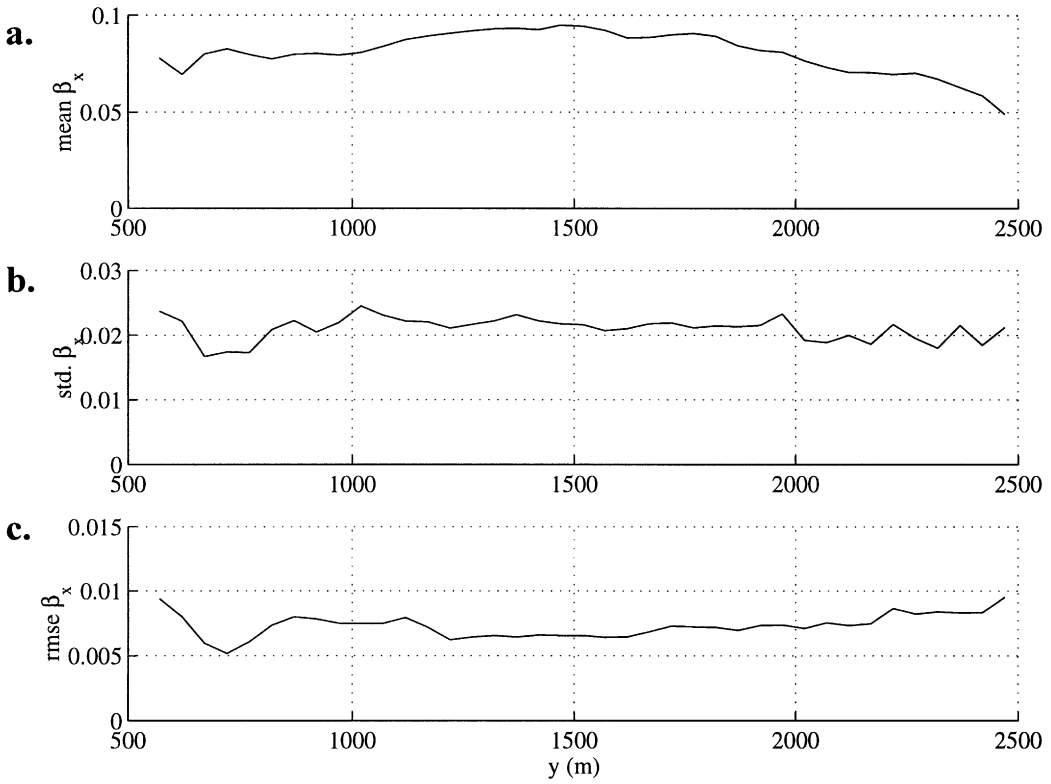


Fig. 6. Beach slope statistics, showing: (a) mean slope, (b) slope standard deviation, and (c) mean estimate error as a function of alongshore location.

$$\beta_x^{ijk}(t) = \hat{\beta}_x^{ijk} + (t - t_i)\dot{\beta}_x^{ijk}, \tag{11c}$$

$$\beta_y^{ijk}(t) = \hat{\beta}_y^{ijk} + (t - t_i)\dot{\beta}_y^{ijk}, \tag{11d}$$

where the hat terms indicate the values of the vertical intercept, cross-shore and alongshore beach slope components at time $t = t_i$ and dot terms are corresponding time-derivatives.

We estimated the beach plate parameters once per day at all alongshore locations and all cross-shore locations of the plan view grid. A weighted linear regression was used, which minimized

$$Q_{\text{plate}}(ijk) = \sum_{i'j'} \{[Z_{\text{plate}}^{ijk}(X_{\text{slim}}\{t_{i'}, y_{j'}\}, y_{j'}, t_{i'}) - \eta(t_{i'})]^2 W_{ii'jj'}\}, \tag{12}$$

The temporal and spatial scales of variability that were resolved were controlled with Loess filter weights, which were defined as

$$W_{ii'jj'} = \begin{cases} [1 - (w_{ii'jj'})^3]^3 & w_{ii'jj'} < 1 \\ 0 & \text{otherwise} \end{cases}, \tag{13}$$

where

$$w_{ii'jj'} = \left[\left(\frac{t_{i'} - t_i}{\lambda_t}\right)^2 + \left(\frac{y_{j'} - y_j}{\lambda_y}\right)^2\right]. \tag{14}$$

$\lambda_t$ is a temporal smoothing scale (set to three days), $\lambda_y$ is the alongshore smoothing scale (100 m). The expected rms error of each of the parameters on the right hand side of Eq. (11b–d) was also computed. Fig. 5 shows an example beach contour map, estimated from the SLIM data set on 23 March 1999.

### 3.3. Description of beach slope variability

While the beach plate parameters were estimated at numerous cross-shore locations, we restricted our

Table 2
Summary of slope estimates over alongshore range $1250 < y < 1750$

| Month | Number | % Selected | Mean | Std. dev. | Alongshore uniformity |
|---|---|---|---|---|---|
| May 1998 | 310 | 84 | 0.097 | 0.026 | 0.63 |
| Aug | 310 | 97 | 0.080 | 0.026 | 0.87 |
| Oct | 310 | 99 | 0.103 | 0.027 | 0.86 |
| Nov | 300 | 86 | 0.100 | 0.024 | 0.96 |
| Dec | 310 | 91 | 0.094 | 0.015 | 0.68 |
| Jan 1999 | 310 | 55 | 0.094 | 0.017 | 0.78 |
| Feb | 280 | 75 | 0.084 | 0.018 | 0.87 |
| Mar | 310 | 100 | 0.089 | 0.020 | 0.94 |

analysis to the cross-shore location that intersected the mean tide level. The slope estimates were interpolated to this location. Hereafter, we omit the cross-shore index, $k$ and focus on alongshore and temporal variations of the slope. Fig. 6 shows time-averaged beach slope statistics at each alongshore location. Some, spatial inhomogeneity is apparent. The mean slope (Fig. 6a) is steepest in the central portion of the study area ($y = 1500$ m), and the standard deviation of the slope (Fig. 6b) was somewhat higher there. The standard deviation computed over all alongshore positions was 0.02. This value (which is about 20% of the mean slope) represents the variation of the beach slope that we want to be able to predict. The expected beach slope sample errors (Fig. 6c) were typically less than 0.01 (mean error was 0.005). The ratio of total variance (i.e. $0.02^2$) to noise variance (i.e. $0.01^2$) was about 4. We can expect that, at most locations, more than 75% of the observed slope variance pertains to actual beach slope variability and 25% may be attributed to sample errors.

Since the model that we wish to test will be forced by wave heights measured at a single location, only alongshore-uniform beach slope changes are consistent with the model assumptions. We decomposed the variability of the beach slope estimates into an alongshore-uniform component and an alongshore-variable component, and we determined their relative contribution to the total temporal variability of the beach slope. The slope decomposition is defined as

$$\hat{\beta}_x(t_i, y_j) = \overline{\hat{\beta}_x}(y_j) + \hat{\beta}'_x(t_i) + \hat{\beta}''_x(t_i, y_j), \qquad (15)$$

where the over bar indicates the time-mean, the single prime denotes the alongshore-uniform residuals about the mean (i.e. the variations that we will compare to the model), and the double prime denotes the residuals due to alongshore variability.

The degree of alongshore uniformity (defined as the ratio $\mathrm{var}[\hat{\beta}'_x]/\{\mathrm{var}[\hat{\beta}'_x] + \mathrm{var}[\hat{\beta}''_x]\}$), was computed monthly over the entire sample area and over a 500 m long sub-region of the study area, which was defined by $1250\ \mathrm{m} \le y \le 1750$ m. In the sub-region, the mean slope (Fig. 6a) was relatively uniform and the expected observation errors were lowest. We found that the degree of alongshore uniformity in this region (Table 2) was relatively high, compared to the value computed over the entire study area. The minimum alongshore uniformity increased from about 0.3 over the full study region to 0.6 across the sub-region. From inspection of the raw images, times of low alongshore uniformity corresponded to times when a sandbar migrated onshore and welded to the shore. The 500 m long sub-region was least affected by this situation.

## 4. Model–data comparisons

### *4.1. Model calibration against observed beach slope changes*

The beach slope model (Eq. (4) with substitution of Eq. (7)) was fit to the observed beach slope changes in the alongshore range ($1250\ \mathrm{m} < y < 1750$ m). The slopes were averaged alongshore, and then the slope changes were estimated from a backward difference. Only cases where slope estimation errors were less than 0.01 were used, which yielded 112 observations. Because the slope observations represent a temporally filtered version of the true slope time series, the input wave forcing variables (i.e. $H$ and $H/L$) were filtered

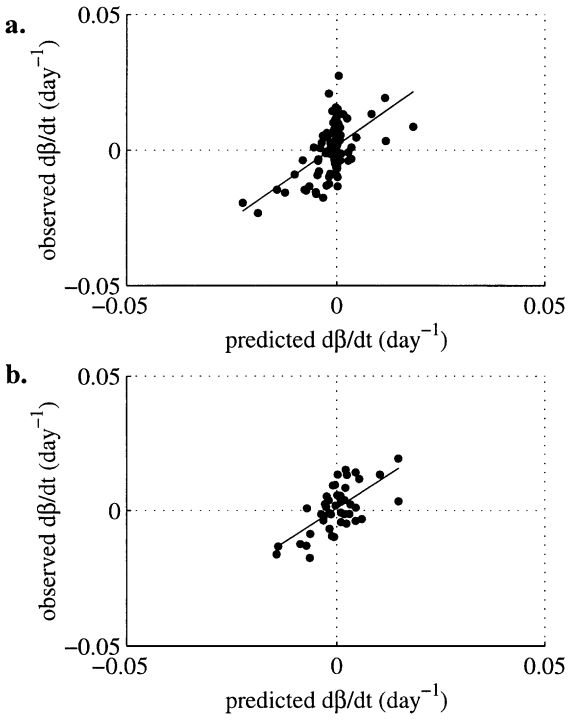


Fig. 7. Observed vs. predicted alongshore-averaged beach slope change rates corresponding to: (a) the entire study period ($R^2 = 0.3$), and (b) the period January through March 1999 ($R^2 = 0.44$). The solid line shows the best linear relationship.

with a three-day loess filter (Eq. (13)). Thus, the analysis did not accurately resolve beach slope variations on time scales shorter than about three days. The model is nonlinear in parameters $a_1$, $a_2$, $p$, $q$, so these parameters were estimated using a nonlinear regression algorithm (Gauss–Newton method), which minimized the mean square error between predicted and observed beach slope change rates. The wave height dependent rate function (term outside square brackets in Eq. (4)) was normalized by the maximum wave height, so that the estimated value of $a_1$ has units of time$^{-1}$ and characterizes the maximum response rate of the system. Likewise, the forcing term $H/L$ in Eq. (7) was normalized by its maximum value.

Fig. 7 compares the predicted and observed slope changes, estimated over the entire record length (Fig. 7a) and over a subset of the record (1 January 1999 through 31 March 1999, Fig. 7b). The skill of the model calibration ($R^2$) over the entire record was 0.30, indicating that the model explained 30% of the observed slope change variance. To test the significance of this skill estimate, we also calibrated the slope change model using random inputs to drive the equilibrium slope term (i.e. $\beta_{eq}$ in Eq. (4) was drawn at random from a population of uniformly distributed values in the range {0, 0.1}). Out of 100 realizations of this random forcing input, each of which contained 112 observations as in the test described above, only 5% of the $R^2$ values exceeded 0.30, suggesting that an $R^2$ value of 0.3 is significant at the 95% level.

The values of the estimated model parameters (Table 3) allow us to interpret several aspects of the dynamics of the beach slope system. Most importantly, the sign of the parameter $a_1$ ($a_1 = -0.52$) was negative, indicating that slopes were driven toward equilibrium. The response time of this system (as indicated by the magnitude of parameter $[a_1]^{-1}$) was about two days, which is shorter than the three-day filter placed on the data. We can assume that the true characteristic response time of the slope system is probably even shorter than two days. The exponent, $p$, was found to be about 4 ($\pm 2$), which is consistent with previous studies. A consistent physical interpretation is that beach slope changes result from a sediment transport rate that increases with the fourth ($\pm 2$)

Table 3
Model–data comparison for sample period May 1998–March 1999

| Forcing (scale) | $N$ | $R^2$ cal. | $a_1$ (95% ci) days$^{-1}$ | $p$ (95% ci) | $a_2$ (95% ci) | $Q$ (95% ci) | $R^2$ pred. | Rms error |
|---|---|---|---|---|---|---|---|---|
| $H/L$ (0.018) | 112 | 0.30 | −0.52 (0.37) | 3.92 (1.90) | 0.16 (0.21) | −2.01 (1.54) | 0.15 | 0.025 |
| [a]$H/L$ (0.018) | 46 | 0.44 | −0.88 (0.81) | 2.21 (1.55) | 0.38 (0.19) | −0.85 (0.54) | 0.33 | 0.015 |
| $H_{rms}$ (1.5 m) | 112 | 0.25 | −0.71 (0.44) | 2.30 (1.26) | 0.57 (0.13) | −0.82 (0.43) | 0.07 | 0.028 |
| $L$ (254 m) | 112 | 0.26 | −0.71 (0.75) | 5.88 (3.11) | 1.54 (1.32) | 2.52 (3.05) | 0.15 | 0.046 |
| $\Omega$ (17) | 112 | 0.31 | −0.67 (0.35) | 3.46 (1.47) | 0.38 (0.21) | −1.95 (1.36) | 0.12 | 0.046 |

[a] Analysis using data from period January 1999–March 1999.

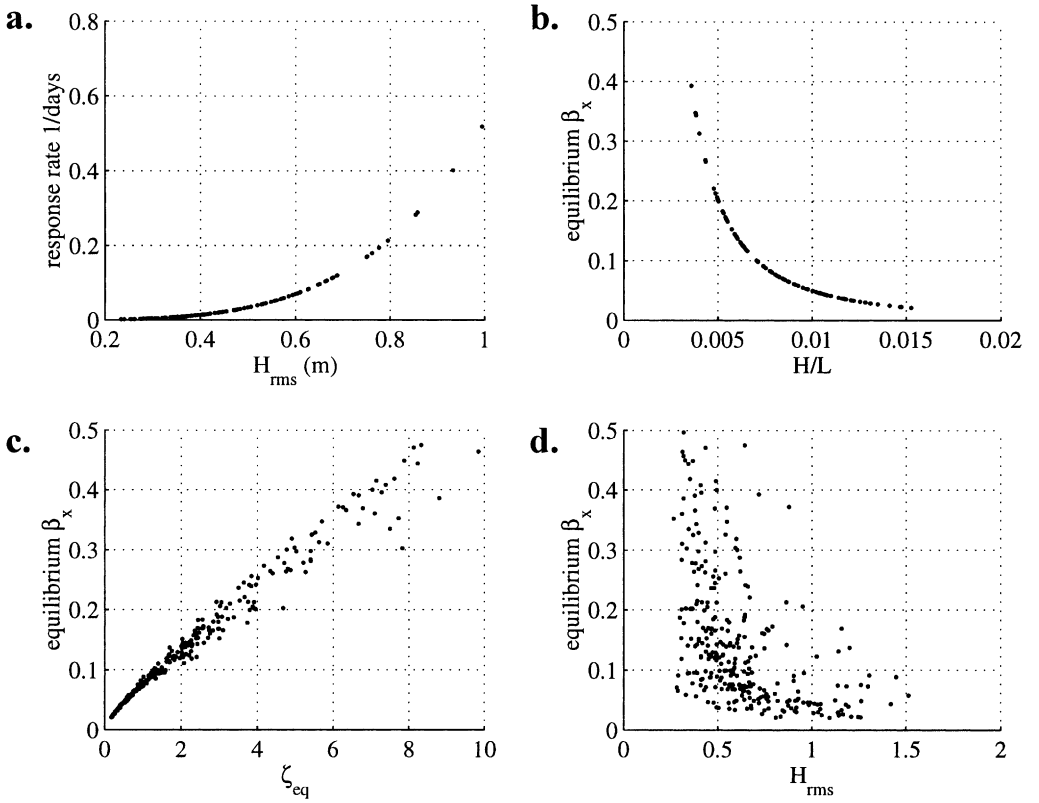


Fig. 8. Calibrated model predictions of: (a) beach slope response rate and (b–d) equilibrium slope as a function of wave steepness, Iribarren number, and wave height.

power of the wave height. Fig. 8a shows the predicted response rate of the system as a function of wave height.

Fig. 8b shows predicted equilibrium slopes as a function of the wave steepness. The predicted equilibrium slope decreases as the steepness increases (because of a negative value in the exponent $q = -2$). This result is consistent with previous studies (where the range of $q$ was $-2$ to $-0.3$, Eqs. (5), (6a) and (6b). If we compare the equilibrium slope predictions to other measures of the hydrodynamics, then we obtain better insight into the role played by the tuning parameters $q$ and $a_2$ ($a_2 = 0.16$). Fig. 8c shows the predicted equilibrium slope as a function of Iribarren number. If the predicted equilibrium slope is 0.1 (approximately the mean slope in the study area), then the corresponding Iribarren number is about 1. This suggests that the average swash zone slope is in equilibrium when hydrodynamic conditions are intermediate between dissipative and reflective conditions.

The results do not, however, suggest that equilibrium slopes always correspond to conditions intermediate between dissipative and reflective. The Iribarren number is a function of wave steepness and the slope (hence the scatter in Fig. 8c). As the wave steepness increases, the predicted equilibrium slope decreases and the Iribarren number at equilibrium also decreases. This has an interesting implication for the feedback between the beach slope and the hydrodynamics. Consider the swash zone slope that is initially in equilibrium. If the wave conditions change abruptly, such that wave steepness increases from its equilibrium value, then the Iribarren number decreases abruptly. The slope that is in equilibrium with the new wave conditions is flatter than the initial slope, so the swash zone slope flattens. This drives the Iribarren number toward still lower values. Thus, the

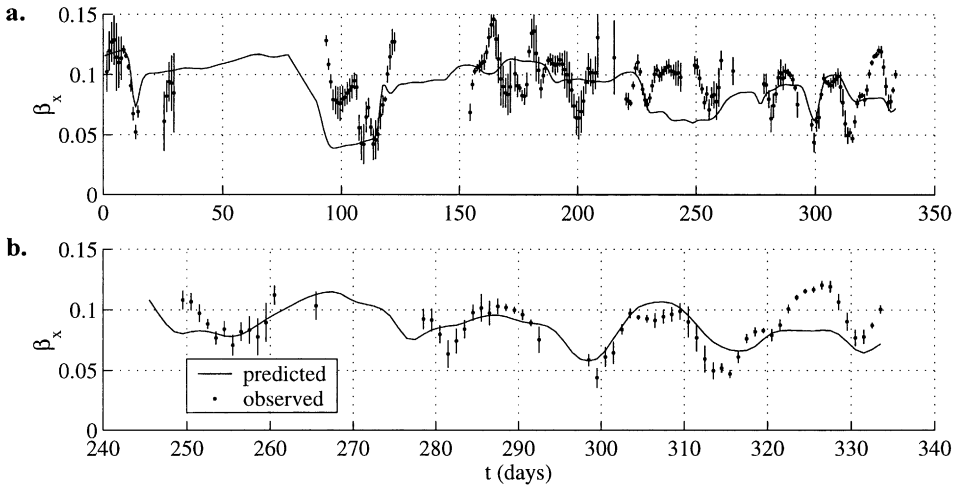


Fig. 9. Time series of observed and predicted slopes, averaged over the region 1250 m $< y <$ 1750 m. The beach slope change model was tuned using: (a) the entire data set, and (b) only the period 1 January 1999–31 March 1999. The model prediction skills were: (a) $R^2 = 0.15$, based on 112 observations, and (b) $R^2 = 0.33$ (46 observations — note time scale change). Error bars on the observations indicate the spatial standard deviation about the alongshore-averaged slope.

morphologic feedback enhances the incident wave field's effect on the local Iribarren number.

### 4.2. Model predictions of beach slope time series

The beach slope model, once calibrated, can be driven with observed offshore wave conditions and used to predict slopes at the shoreline. The model is stable because the slope is always driven toward the equilibrium value. We predicted the alongshore-averaged (within the 500 m long sub-region) beach slope. Fig. 9 shows several example slope predictions, initialized with the first observed slope value. The predictions in both examples were significantly correlated to the observed slope variations (15% and 33% of variance explained). However, in the case of Fig. 9a, the rms prediction error (0.025, Table 3) was roughly equal to the beach slope standard deviation of 0.021 (Fig. 6b). Thus, approximately the same rms prediction error would result from predicting that the slope is always equal to the time-mean slope. In the second example (Fig. 9b), the model performed better, with an rms prediction error of 0.015.

As Table 3 indicates, we drove the model with various other forcing variables, including wave height alone (i.e.$\beta_{eq} = a_2\{H_{rms}\}^q$), wave length alone, and Dean's parameter. The largest calibration skill (prediction of slope changes between consecutive one-day periods) and largest slope prediction skill (prediction of the alongshore-averaged slope time series) was found for the model whose equilibrium term was forced by wave steepness. The model forced by only wave height or only wave length, or by $\Omega$ had similar calibration skills, but significantly larger rms error of the time series predictions.

## 5. Discussion

### 5.1. Modeling errors

The model comparison presented here gave insight into observed beach slope dynamics when the model was used to constrain unknown model parameters. However, it appears that these dynamics are not necessarily parameterized accurately enough to make reliable beach slope forecasts. It is likely that the predictions suffered because we calibrated the model against slope changes, rather than fitting to the slopes themselves. This calibration approach emphasizes the high-frequency components of the slope time series, which does not optimize the model predictions over long time periods.

The present model for equilibrium slope prediction

(Eq. (7)) cannot be consistent with natural beaches over the full range of forcing conditions. For instance, in the low wave steepness limit the model predicts an infinitely steep beach slope. The model inconsistency is, however, masked by the wave-height dependence in the response rate (Eq. (4)). If the wave steepness decreases due to a decreasing wave height, then the response rate also decreases. The response rate is zero when the wave height is zero and predicted beach response becomes insensitive to the beach slope disequilibrium. If we wish to make accurate predictions, then it is probably never necessary to specify an equilibrium slope formulation that is correct for the case of relatively small wave heights. Fig. 8d illustrates this point, indicating the steepest and least realistic predicted equilibrium slopes occur at low wave heights.

A better formulation for the equilibrium slope should come from a direct analysis of sediment transport processes in the swash zone. In analogy to Bowen's (1980) analysis of the region seaward of the swash zone, a process-based equilibrium slope prediction will result from a computed balance between down slope transport and up slope transport, averaged over several wave or tide cycles. It is possible, although perhaps unlikely, that such a balance could exist in the presence of net onshore or offshore transport. It is not clear how the present steepness-based parameterization accounts for this balance. Additionally, geometrical inspection of the beach slope problem shows that more sediment transport is required to change a flat slope (corresponding to a wide swash zone) compared to changing a steep slope. The slope response rate must depend on both forcing conditions and the inverse of the slope squared, providing mass is conserved.

Because we used offshore incident wave height to estimate the forcing, the forcing at the shore is probably not accurately predicted, particularly during high-energy periods when waves break far from shore. However, the forcing at the shore is certainly related to the forcing offshore, albeit in a nonlinear relationship that depends on the details of the intervening bathymetry. For instance, under conditions of high wave steepness (or low Iribarren numbers), wave breaking will drive setup and low-frequency wave motions at the shore (Guza and Thornton, 1985). Beach flattening (or at least offshore transport) in the swash zone has been associated with both increased water levels within a tidal cycle (Duncan, 1964) and increased low-frequency wave energy (Butt and Russel, 1999).

Finally, the presence of non-uniform morphology in the alongshore direction hampered our efforts to test the originally posed model, which pertained to the behavior of a spatially uniform beach slope in response to spatially uniform forcing. Instead, we have compared the model to an intertidal beach that experienced considerable alongshore variability. For instance, in May 1999 as little as 63% of the observed beach slope variability was alongshore uniform within the 500 m test section (only 28% of the variations were alongshore-uniform over the full 2 km study area). The observed morphologic variability in the alongshore direction was certainly coupled to hydrodynamic variability in the alongshore direction, most likely as a result of interactions with the nearshore bar. This interaction folded itself into our model–data comparison and model parameter estimations in an unknown manner. We dealt with this problem, in part, by restricting our analysis to a sub-region of the originally sampled study area. Additionally, we analyzed a temporal subset of the data (January 1999–March 1999), which was selected to minimize the effect of changing offshore morphology. The model calibration and prediction skills improved significantly and the model parameters varied by less than a factor of 2 and, more importantly, they did not change sign (Fig. 7b, Table 3). This suggests that our interpretations of the results are robust.

## 6. Conclusions

This paper presented a test of a very simple model that predicts beach slope changes. The model assumes that these changes are a function of the incident wave conditions and the beach slope itself. Following other beach morphology studies, we hypothesized that the beach slope evolves towards an equilibrium value that depends nonlinearly on wave steepness. The rate of beach slope response is assumed to be a function of the degree of slope disequilibrium and the incident wave height, raised to some power.

The model was tested against beach slope variations derived from digital images of the nearshore

zone. Approximately, $10^4$ images were analyzed in order to extract the location of the shoreline. From these images, nearly $10^5$ shoreline position estimates were obtained over eight different month-long periods (which were generally consecutive) along a 2 km length of the beach. These data were used to estimate the beach slope once per day over the study period. In order to obtain uniformly accurate slope estimates, each estimate utilized data within $\pm 3$ days and $\pm 100$ m (alongshore) of the time–space coordinates of the estimation point, yielding approximately 6000 beach slope estimates.

The model predictions of a slope that evolved toward a time-varying equilibrium were consistent with the beach slope observations. The best of several competing models was that which assumed that the equilibrium slope was proportional to the wave steepness ($H/L$) raised to the power $-2$. The inverse relationship indicates that beaches were driven toward flatter slopes when the wave steepness was large, and vice versa. This result is generally consistent with earlier models, based on static comparisons between slope and wave conditions. Our model comparison indicated that the response rate of the slope depended on the wave height, raised to the fourth power. A characteristic response time for the system was found to be 1–2 days, which is probably an overestimate in light of the temporal smoothing imposed by the slope estimation procedure.

When the model was calibrated to fit the observed one-day changes in beach slope, the predicted slope changes explained 30 and 40% of the observed slope-change variance. The calibrated model was used to predict time series of beach slope evolution. The rms error between slope prediction and slope observations was equal to or only slightly lower than the observed temporal variability in the slopes. Thus, while the calibration stage of this analysis indicates that the model is consistent with the observations, the present model is not sufficiently accurate to outperform a model that predicts a slope equal to the mean slope.

These results call into question the accuracy of attempts that use existing simple models to predict anything but geographic variations in beach slope. Rather than having general applicability, simple slope prediction models may be able to make statistically significant predictions only under conditions of: (i) relatively simple intertidal morphology (e.g. alongshore uniformity), (ii) relatively simple and constant morphology seaward of the intertidal zone, and (iii) constant grain sized distribution. This statement implies that the simple models must be re-calibrated as (i)–(iii) change, so that these changes can be absorbed into the model coefficients.

## Acknowledgements

Funding for this work was provided by University of Twente, Faculty of Technology and Management, Department of Integrated Modeling (MICS) to support A. Madsen. N. Plant was supported by the United States' Office of Naval Research through its NICOP project grant no. N00014-97-1-0793, PR no. 97PR184-00. The video images were generously supplied by Rob Holman at Oregon State University's Coastal Imaging Lab. The survey, wave, and tide data were supplied by US Army Corps of Engineers' Field Research Facility. We are grateful to the international members of the ARGUS group for their role in the development of video imaging analysis ideas and tools. We thank the two reviewers for their comments.

## Appendix A. Quality control

To control the accuracy of the data that were used to test the beach slope evolution model (Eq. (4)), we implemented two stages of quality control. The first stage related to the errors associated with extracting the SLIM feature form the image data. Errors were encountered at this stage primarily because of image to image variability that hampered our attempts to accurately identify the SLIM as a shoreline proxy. The second stage of quality control related to the errors associated with sample beach slope estimates. These errors depended on residual errors in the SLIM identification as well as other errors associated with fitting the articulated beach plates (Eq. (11a)) to the observations.

### *A.1. SLIM extraction quality control*

Quality control constraints were applied interactively within the SLIM identification algorithm (Fig. 4). The interactive control ensured that only

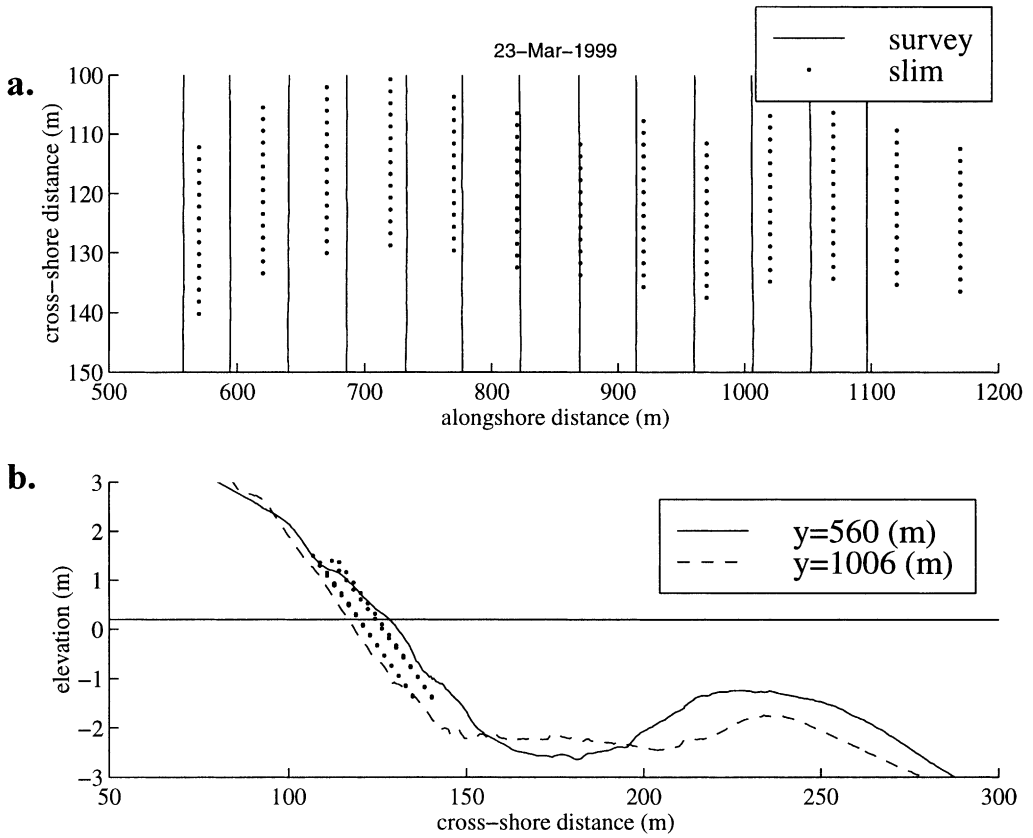


Fig. A1. (a) Spatial distribution of SLIM shoreline position estimates and CRAB survey on 23 March 1999. (b) Comparison of surveyed bathymetry at two alongshore locations. The mean tide level is shown as a solid line.

confidently estimated SLIM positions were used to 'teach' the initialization function (Eq. (10)) about the spatial and temporal variations of the SLIM. These constraints required that the estimated width of the SLIM, $L_{slim}$, exceeded the width of 95% confidence interval ($L_{ci}$) of the estimate (i.e. the true SLIM width likely to be larger than zero width). Also, the 95% confidence interval about the SLIM position was required to be less than the SLIM width. Finally, the SLIM position itself was required to lie within $3Q^{1/2}$ of the initial guess (i.e. three times the standard deviation of the initialization model's residuals). These constraints prevented contamination of the identification procedure by extremely anomalous observations.

Once all SLIM positions had been estimated, these data were passed through a more detailed set of selection criteria. The selection criteria are presented in Table 1. The aim of this stage of analysis was to utilize both physical constraints and statistical constraints to eliminate further spurious observations. Because of the very large sample size ($N \sim 10^4$ per month), it was impractical to visually inspect all of the SLIM positions superimposed on their corresponding plan images (i.e. Fig. 3a). However, we inspected histograms of the SLIM identification function parameters. We expected these histograms to be single-peaked and centrally distributed. The final choices of selection criteria shown in Table 1 are the end result of iteratively choosing criteria and inspecting the resulting histograms. We attempted to strike a balance between overly strict criteria (which would leave us with too few data for beach slope estimation) and overly lenient criteria (which would include too many spurious data). We maintained a high level of objectivity throughout the image analysis by relying

heavily on equations (Eqs. (9) and (10)) to encode our expectations.

### A.2. Beach slope sample quality control

We implemented quality control measures to ensure that the articulated beach plate parameters were accurately estimated. Reasons to reject particular estimates included poor correlation between SLIM positions and the tide level, or too few SLIM estimates to adequately constrain the beach plate parameters. An estimate was rejected if the expected rms error of the local elevation (i.e. $\hat{z}_0^{ijk}$, Eq. (11b)) exceeded 0.1 m. To compute the expected error (Priestley, 1981, p. 368), the sample size corresponding to each estimate was assumed to equal the sum of the weights, $w_{ii'jj'}$ (Eq. (14)). Also, an estimate was rejected if the expected error of the local cross-shore slope (i.e. $\hat{\beta}_x^{ijk}$, Eq. (11c)) exceeded 0.01.

### A.3. Comparison to in situ surveys

In order to check that the SLIM-derived slope estimates were accurate, we made use of monthly bathymetric surveys, conducted at the FRF site. The surveys were obtained using GPS survey equipment, mounted on the 10 m tall Coastal Research Amphibious Buggy (CRAB). The vertical survey accuracy of these data is about 10 cm. A total of eight survey dates were available for comparison. The surveys traversed several cross-shore transects, spaced approximately 40 m apart in the alongshore direction (Fig. A1). We used 13 cross-shore CRAB transects, which were within 50 m in the alongshore direction of the SLIM data.

The CRAB data were used to constrain the beach plate parameters (Eq. (11a)–(11d)) in nearly the same manner as the SLIM data. The only difference in the CRAB data analysis was the omission of the temporal derivative terms in Eq. (11b)–(11d). The mean difference between the CRAB and SLIM elevation estimates was −0.12 m, indicating that, on average, the SLIM based elevation estimates lay above the surveyed bathymetry. This is consistent with the magnitude of vertical offset found by PH97. The standard deviation about the mean error was 0.17 m. The mean difference in the cross-shore slope estimates was −0.01, indicating that the SLIM slope estimates tended to over-estimate the CRAB-surveyed slopes by about 10% of the mean slope. Finally, the standard deviation of the slope differences, computed over all samples, was 0.014. The rms error (0.017) is nearly the same as the observed temporal variation of the beach slopes (Fig. 6b). However, some portion of the errors presented here must be attributed to actual differences in the morphology, since the spatial and temporal sampling schemes of the CRAB and SLIM data sets differed. Thus, the actual errors between the SLIM data and the true intertidal morphology are most likely smaller than those presented here.

The differences in slope estimates obtained using the two data types appear to be related to the proximity of the sandbar to the shoreline. As the bar approaches the shoreline, it interferes with the generation of a distinct SLIM. Also, when the bar is close to the shoreline, it may be exposed at low tide. Identifying it as the SLIM may in fact result in a locally accurate estimate of the nearshore bathymetry. Under these circumstances, however, the trough landwards of the bar will not be identified from the SLIM data, while it is well identified using the CRAB data. The intertidal slopes estimated from the SLIM data will tend to be too flat when compared to the CRAB data.

## References

Bascom, W., 1954. Waves and Beaches. Anchor Books, Garden City, NY.

Battjes, J.A., 1974. Surf similarity. In: Proceedings of the 14th International Conference on Coastal Engineering, ASCE, pp. 446–480.

Birkemeier, W.A., 1985. Time scales of nearshore profile change. In: Proceedings of the 19th International Conference on Coastal Engineering, ASCE, New York, pp. 1507–1521.

The CRAB, Birkemeier, W.A., Mason, C., 1984. A unique nearshore surveying vehicle. J. Surv. Engng 110, 1–7.

Birkemeier, W.A., Miller, H.C., Wilhelm, S.D., DeWall, A.E., Gorbics, C.S., 1985. User's guide to CERC's Field Research Facility, Coastal Eng. Res. Cent., Field Res. Fac., U. S. Army Eng. Waterw. Exp. Sta., Vicksburg, Miss.

Bowen, A.J., 1980. Simple models of nearshore sedimentation: beach profiles and longshore bars. The Coastline of Canada, McCann, S.B. (Ed.), Geol. Surv. Can. Ottawa (Paper 80-10), 1–11.

Butt, T., Russel, P., 1999. Suspended sediment transport mechanisms in high-energy swash. Mar. Geol. 161, 361–375.

Dalrymple, R.A., Thompson, W.W., 1976. Study of equilibrium beach profiles. In: Proceedings of 15th Coastal Engineering Conference, ASCE, pp. 193–200.

Dean, R.G., 1973. Heuristic models of sand transport in the surf zone. In: Conference on Engineering Dynamics in the Surf Zone, ASCE, Sydney, NSW, pp. 209–214.

Duncan, J.R.J., 1964. The effects of water table and tide cycle on swash-backwash sediment distribution and beach profile development. Mar. Geol. 2, 186–197.

Guza, R.T., Thornton, E.B., 1985. Observations of surf beat. J. Geophys. Res. 90 (C2), 3161–3172.

Harrison, W., 1969. Empirical equations for foreshore changes over a tidal cycle. Mar. Geol. 7, 529–551.

Holland, K.T., Holman, R.A., 1996. Field observations of beach cusps and swash motions. Mar. Geol. 134, 77–93.

Holland, K.T., Holman, R.A., Lippmann, T.C., Stanley, J., Plant, N., 1997. Practical use of video imagery in nearshore oceanographic field studies. IEEE J. Ocean. Engng 22 (1), 81–92.

Holman, R.A., Sallenger Jr., A.H., 1993. Sand bar generation: A discussion of the Duck experiment series. J. Coastal Res. (15), 76–92 (Special issue).

Komar, P.D., 1998. Beach Processes and Sedimentation. Prentice-Hall, New Jersey, p. 544.

Kriebel, D.L., Dean, R.G., 1993. Convolution method for time-dependent beach-profile response. J. Waterways, Port, Coastal, Ocean Engng 119 (2), 204–226.

Lippmann, T.C., Holman, R.A., 1989. Quantification of sand bar morphology: a video technique based on wave dissipation. J. Geophys. Res. 94 (C1), 995–1011.

Lippmann, T.C., Holman, R.A., 1990. The spatial and temporal variability of sand bar morphology. J. Geophys. Res. 95 (C7), 11 575–11 590.

Lippmann, T.C., Holman, R.A., Hathaway, K.K., 1993. Episodic, non-stationary behavior of a two sand bar system at Duck, NC, USA. J. Coastal Res. (15), 49–75 (Special issue).

Miller, J.R., Miller, S.M.O., Torzynski, C.A., Kochel, R.C., 1989. Beach cusp destruction, formation, and evolution during and subsequent to an extratropical storm, Duck, North Carolina. J. Geol. 97, 749–760.

Nichols, R.J., Birkemeier, W.A., Lee, G., 1998. Evaluation of depth of closure using data from Duck NC, USA. Mar. Geol. 148, 179–201.

Plant, N.G., Holman, R.A., 1997. Interannual shoreline variations at Duck, NC, USA. In: Proceedings of the 25th International Conference Coastal Engineering, pp. 3521–3533.

Plant, N.G., Holman, R.A., 1997b. Intertidal beach profile estimation using video images. Mar. Geol. 140, 1–24.

Plant, N.G., Holman, R.A., Freilich, M.H., Birkemeier, W.A., 1999. A simple model for interannual sandbar behavior. J. Geophys. Res. 104 (C7), 15 755–15 776.

Priestley, M.B., 1981. Spectral Analysis and Time Series, 890. Academic Press, London, p. 890.

Sunamura, T., 1984. Quantitative predictions of beach-face slopes. Geol. Soc. Am. Bull. 95, 242–245.

Thornton, E.B., 1979. Energetics of breaking waves within the surf zone. J. Geophys. Res. 84, 4931–4938.

Wright, L.D., Short, A.D., 1984. Morphodynamic variability of surf zones and beaches: a synthesis. Mar. Geol. 56, 93–118.

Wright, L.D., Short, A.D., Green, M.O., 1985. Short-term changes in the morphodynamic states of beaches and surf zones: an empirical predictive model. Mar. Geol. 62, 339–364.